Dipole engineering in self-assembled monolayers for efficient organic–silicon hybrid solar cells

View Online   Export Citation   CrossMark

Zhangbo Lu,[a] [ID] Jiahui Chen, Yueyue Wu, Huanyu Wen, Dan Chi, and Shihua Huang[a]

AFFILIATIONS

Key Laboratory of Solid State Optoelectronic Devices of Zhejiang Province, College of Physics and Electronic Information Engineering, Zhejiang Normal University, Jinhua 321004, China

[a]Authors to whom correspondence should be addressed: luzhangbo@zjnu.edu.cn and huangshihua@zjnu.cn

ABSTRACT

Organic–silicon hybrid solar cells, as dopant-free heterojunction devices, hold significant potential for achieving high performance-to-cost ratios in photovoltaics. Critical to their advancement is the engineering of carrier-selective contacts that minimize interfacial losses. Here, we demonstrate a carbazole-based self-assembled monolayer (SAM), [4-(3,6-dimethyl-9H-carbazol-9-yl)butyl]phosphonic acid (Me-4PACz), as an efficient electron-selective layer in [poly(3,4 ethylenedi oxythiophene):polystyrene sulfonate (PEDOT:PSS)]/Si solar cells. The Me-4PACz SAM introduces a directional dipole moment at the c-Si/Al interface, generating a built-in electric field that enhances electron extraction. This interface modification leads to a linear Ohmic contact, reducing the contact resistivity between n-Si and the metal electrode interface to $4.12 \, \mathrm{m\Omega \, cm^2}$. Consequently, the optimized device achieves a power conversion efficiency (PCE) of 16.75% with a high open-circuit voltage (V_{OC}) of 651 mV and fill factor of 78.03%, representing a ~14% relative PCE improvement over the control device (PCE = 14.75%). Our work provides a molecular-scale strategy for tailoring carrier dynamics in silicon-based heterojunctions, offering a pathway toward low-cost, high-efficiency photovoltaic technologies.

Published under an exclusive license by AIP Publishing. https://doi.org/10.1063/5.0286438

As the global energy structure transformation deepens, solar cell technology has drawn significant attention as the core carrier for the utilization of renewable energy. Up to now, crystalline silicon (c-Si) photovoltaic devices have achieved full commercialization, dominating the photovoltaic field with a market share exceeding 95%. Among them, the power conversion efficiency (PCE) of crystalline silicon (c-Si) solar cells with interdigitated back contact (IBC) heterojunction (HJT) structures has exceeded 27%.[1,2] Despite the impressive efficiency of HJT-IBC solar cells, their large-scale development has been hindered by both capital-intensive and cost-intensive factors. Meanwhile, HJT devices suffer from high optical losses, primarily attributed to the severe parasitic light absorption in the doped hydrogenated amorphous silicon layers.

Against this backdrop, organic–silicon hybrid solar cells have emerged as a pivotal development pathway for next-generation photovoltaic technologies. By implementing dopant-free heterojunction integration of organic semiconductors and inorganic silicon substrates, these devices demonstrate synergistic advantages, including high carrier mobility, tunable light absorption spectra, and superior solution processability compatible with roll-to-roll manufacturing.[3–6] Of particular interest is the PEDOT:PSS/Si hybrid architecture,[7–10] which has garnered substantial research attention due to its low-temperature

process compatibility (<150 °C), interface energy-level tunability via molecular dipole engineering, and recorded PCE exceeding 18.3% in proof-of-concept devices.[11]

However, the charge recombination effect and energy-level mismatch at heterogeneous interfaces severely restrict the improvement of device performance. Research has shown that the electronic selectivity of the interface contact layer has a decisive influence on the efficiency of carrier extraction. Specifically, low-work function metal oxides and fluorides (e.g., TiO_2, TaO_X, ZnO, LiF, and MgF_2) have been demonstrated as electron-selective contacts,[12–18] effectively facilitating electron extraction and transport at the metal electrode/c-Si interface to achieve high-performance photovoltaic devices. However, these approaches suffer from inherent limitations: their high-temperature annealing processes (>300 °C) exhibit poor compatibility with organic components. Furthermore, the ultrathin electron transport layers requiring precise thickness control necessitate high-precision deposition techniques such as atomic layer deposition, escalating manufacturing costs and process complexity, thereby presenting significant challenges for large-scale production. In recent years, self-assembled monolayers (SAMs) technology has been employed to precisely modulate the interface energy-level configuration at the nanoscale via the chemical bonding between molecular end functional

groups and substrates. Its distinctive molecular orientation and orderliness are beneficial for constructing efficient charge transfer channels. For instance, phosphate-based SAMs have shown outstanding hole transport capacity in perovskite solar cells,[19–25] but systematic research on organic/silicon heterojunction photovoltaic systems remains insufficient.

　　In this work, SAMs of [4–(3,6-dimethyl-9H-carbazol-9-yl)butyl]-phosphonic acid (Me-4PACz) are employed as electron-selective contacts in PEDOT:PSS/Si solar cells. By introducing Me-4PACz, directional dipole moments are engendered at the c-Si/Al interface, facilitating effective electron extraction. Following the deposition of Me-4PACz, the Schottky barrier at the c-Si/Al interface was suppressed, achieving an obviously reduction in interfacial contact resistivity to $4.12\,\mathrm{m\Omega\,cm^2}$. Consequently, the PEDOT:PSS/Si hybrid solar cell with the Me-4PACz SAM-based electron-selective interlayer attained an efficiency of 16.7%, featuring a high open voltage (V_{OC}) of 651 mV and a high fill factor (FF) of 78.03%.

　　When Me-4PACz was spin-coated onto a [Tetramethylammonium hydroxide (TMAH)]-treated c-Si surface, it formed multilayered SAMs. The bottom-layer SAM chemically adsorbs onto the surface [oxhydryl (OH)] groups of TMAH-treated c-Si with strong bonding, while the upper-layer SAM is only weakly bonded through physical adsorption, leading to dissociation after isopropanol rinsing.[19,26,27] The relevant deposition and dissociation processes are depicted in Fig. 1(a). A single molecule of Me-4PACz is composed of non-polar carbazole groups and polar phosphate groups, featuring a distinct chemical structure as depicted in Fig. 1(b). To obtain direct evidence related to the existence of Me-4PACz-related atomic species on the c-Si surface, x-ray photoelectron spectroscopy (XPS) was utilized to detect the SAM-coated

substrates. Among them, the high-resolution XPS spectroscopy testing of P 2p and N 1s (Fig. S1), along with the contact angle testing (Fig. S2), jointly confirmed the existence of Me-4PACz SAM. In addition, as illustrated in Figs. S3 and S4 (supplementary material), the atomic force microscopy (AFM) topographic and Kelvin probe force microscopy (KPFM) surface potential mapping collectively demonstrate that the Me-4PACz monolayer exhibits a uniform distribution on the c-Si substrate surface. These findings not only confirm the construction of the SAM on the silicon interface but further reveal that the SAM possesses good surface coverage. Figures 1(c) and 1(d) exhibit the high-resolution C 1s binding energy regions of c-Si and c-Si/SAM substrates, respectively. The C 1s signal at 284.8 eV in bare n-Si is attributed to adventitious carbon contamination from ambient exposure. Notably, the c-Si/SAM substrate additionally shows characteristic signals of Me-4PACz and its carbazole components. In addition, the high-resolution XPS spectra of the Si 2p core energy levels for both the bare c-Si and c-Si/Me-4PACz samples were also characterized, as depicted in Figs. 1(e) and 1(f). In contrast to bare c-Si, the Si-OH peak exhibited a decrease after SAM coating, indicating that the silicon hydroxyl groups on the c-Si surface underwent a condensation reaction and chemically interacted with the phosphate groups of Me-4PACz. Eventually, bonds such as Si–O–P or Si–OH–P might be formed at the c-Si/Me-4PACz interface.[28]

　　Low contact resistivity (ρ_c) can efficaciously diminish the Ohmic losses and potential barriers at the interface between c-Si and carrier-selective contacts, facilitate efficient carrier transport, and conspicuously enhance the optoelectronic performance of solar cells. To acquire the ρ_c of the SAM-modified n-Si/Al interface, the transmission length method (TLM) was utilized for measurement.[29] The lateral transmission test structure of the TLM method is conspicuously depicted in
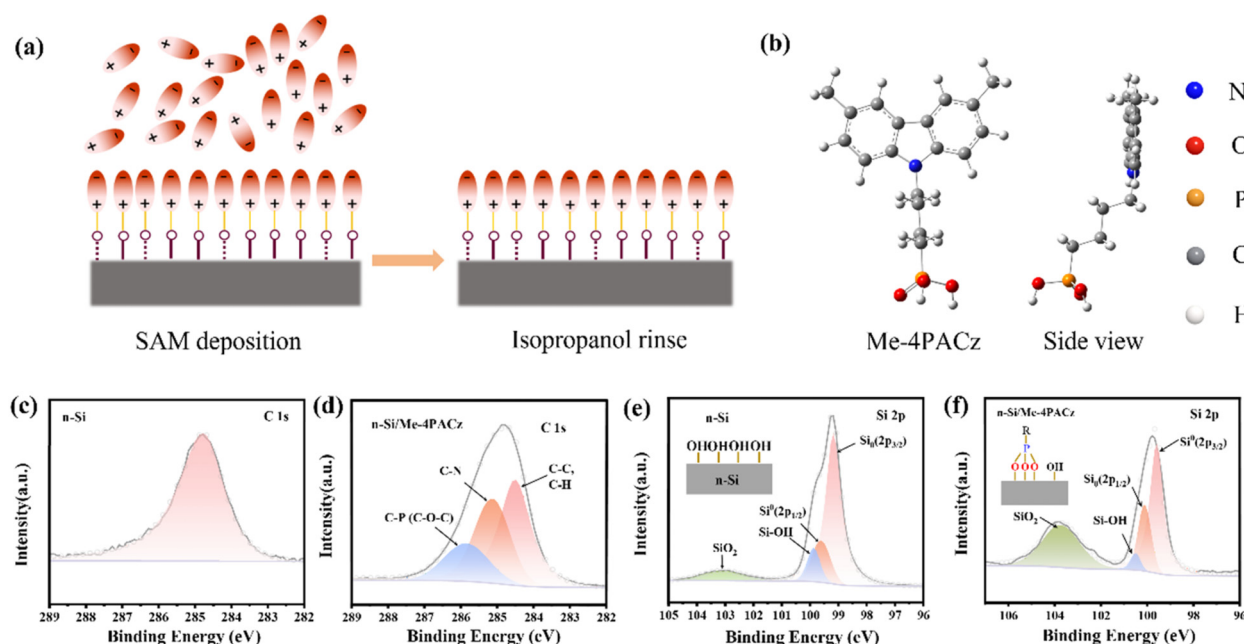
FIG. 1. (a) Schematic illustration of the adsorption and desorption process of SAM on c-Si surface rinsed with isopropanol. The dotted line indicates a weak hydrogen bond. (b) Molecular structure and side view of Me-4PACz. High-resolution XPS spectra of C 1s for (c) n-Si and (d) n-Si/Me-4PACz. High-resolution XPS spectra of Si 2p region for (e) n-Si substrate and (f) n-Si/Me-4PACz.
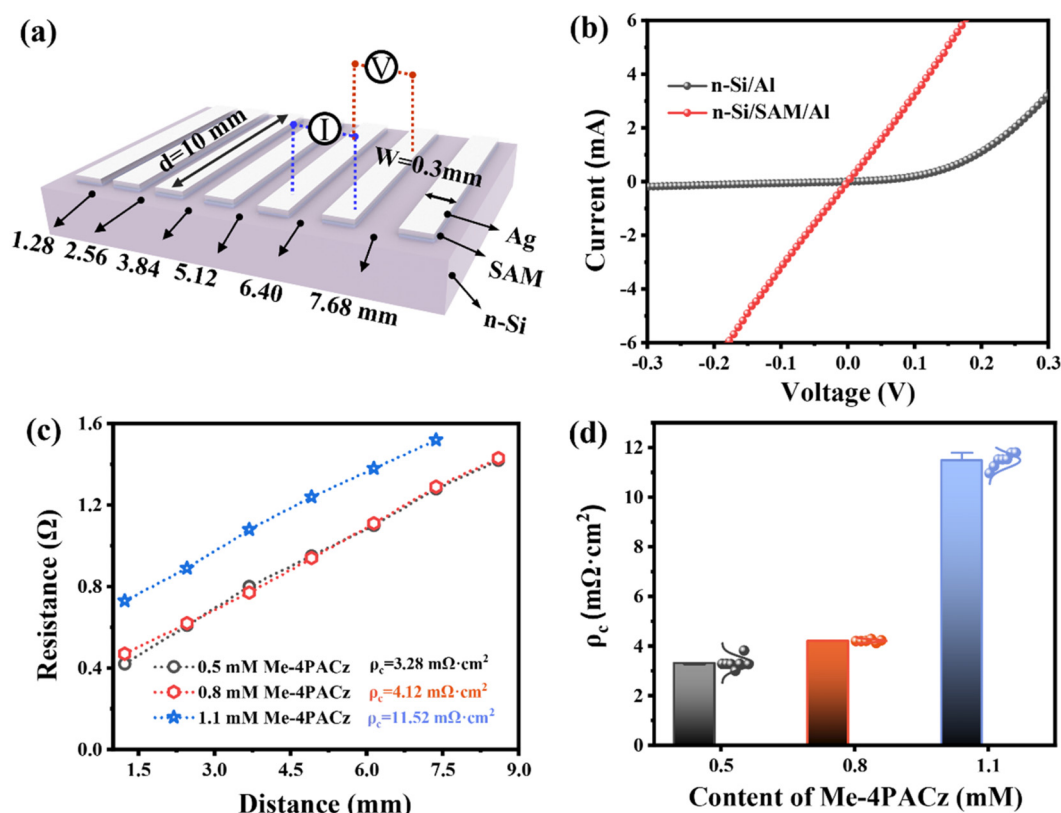
FIG. 2. (a) Schematic diagram of n-Si/SAM/Al contact structure extracted from ρ_c based on the TLM method. (b) Dark I–V measurement of samples based on n-Si/Al and n-Si/SAM/Al structures. (c) Plots of R_T vs L and the corresponding linear fitting curves. (d) ρ_c of n-Si/SAM/Al contacts with different concentrations of Me-4PACz. Seven individual samples were measured for each Me-4PACz concentration indicated in the solid sphere.

Fig. 2(a). Figure 2(b) depicts the dark I–V curves of the n-Si/Al and n-Si/SAM/Al structures. In contrast to the typical Schottky characteristics of n-Si/Al contacts, n-Si/SAM/Al contacts demonstrate linear Ohmic transport properties, suggesting that the SAM layer mitigates the Fermi level pinning effect induced by metal-induced interstitial states via interface dipole modulation, which is in accordance with the results presented in Fig. 3. The corresponding graphs of total resistance (R_T) and length (L) of n-Si/SAM/Al interfaces modified with diverse concentrations of Me-4PACz, along with the linear fitting curves, are depicted in Fig. 2(c). Among them, the minimum value of extracted ρ_c and the results of displaying the concentration of each Me-4PACz for seven individual samples are shown in Figs. 2(c) and 2(d), respectively. In the concentration gradient experiment of Me-4PACz (0.5–1.1 mM), as the concentration of Me-4PACz rose from 0.5 to 0.8 mM, the minimum value of extracted ρ_c slightly ascended from 3.28 to 4.12 mΩ cm^2. This trade-off between ρ_c and passivation reflects SAM coverage effects. The contact angle jump (80.59° → 85.10°, Fig. 2) confirms transition from partial coverage (0.5 mM) enabling localized low ρ_c but poor passivation, to near-complete monolayer (0.8 mM) providing uniform dipole functionality and effective passivation that maximizes PCE despite slightly higher ρ_c. When the concentration reached 1.1 mM, the ρ_c sharply soared to 11.52 mΩ cm^2. This phenomenon might be associated with the interface dipole disorder caused by π–π

stacking among SAM molecules at high concentrations.[30,31] Nevertheless, all the ρ_c values are still conspicuously lower than the series resistance values of most c-Si solar cells.[16,18,32–34]

To elucidate the electronic structure regulation mechanism of Me-4PACz on the Al electrode, the electric dipole moment and electrostatic potential distribution of Me-4PACz molecules were obtained based on Gaussian 16 quantum chemistry calculations [Fig. 3(a)]. The asymmetric charge characteristics thereof indicate the existence of an intrinsic dipole moment of up to 3.32 Debye within the molecule, which is aligned with the charge separation direction from the phosphonic acid group (positively charged) to the carbazole group (negatively charged), suggesting the formation of a directional dipole layer at the metal/semiconductor interface. Meanwhile, kelvin probe force microscopy (KPFM) analysis revealed that the Me-4PACz modification enhanced the average surface potential of the n-Si/Al interface by 334 mV, which was equivalent to a decrease in the work function of the Al electrode from 4.55 to 4.24 eV [Figs. 3(b) and 3(c)]. The trend was further validated by ultraviolet photoelectron spectroscopy (UPS) testing, and it was discovered that the work function of Al significantly dropped from 4.05 to 3.75 eV [Fig. 3(d)]. It is notable that although there exists a systematic deviation in the absolute work function values between the two methods due to the disparities in the testing environment (atmosphere/vacuum) and principle, the difference in the work
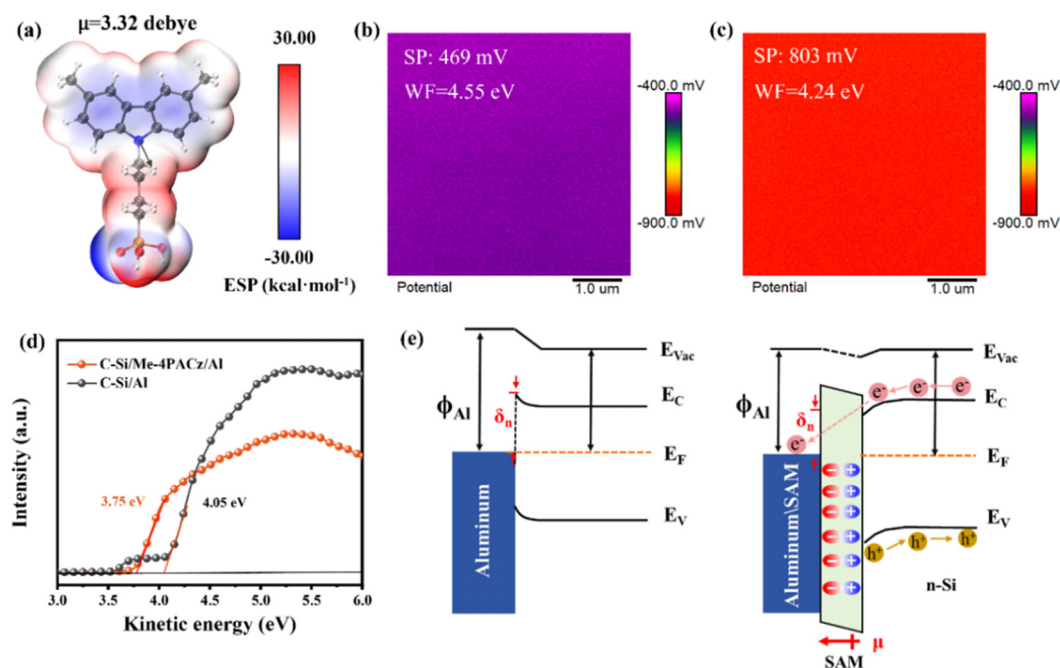
FIG. 3. (a) and (b) KPFM mapping images of n-Si/Al and n-Si/Me-4PACz/Al films. (c) UPS measurements for a n-Si/Al and n-Si/Me-4PACz/Al. (d) Electrostatic potential and dipole moment of Me-4PACz. (e) Band arrangement of n-Si/Al and n-Si/Me-4PACz/Al junctions.
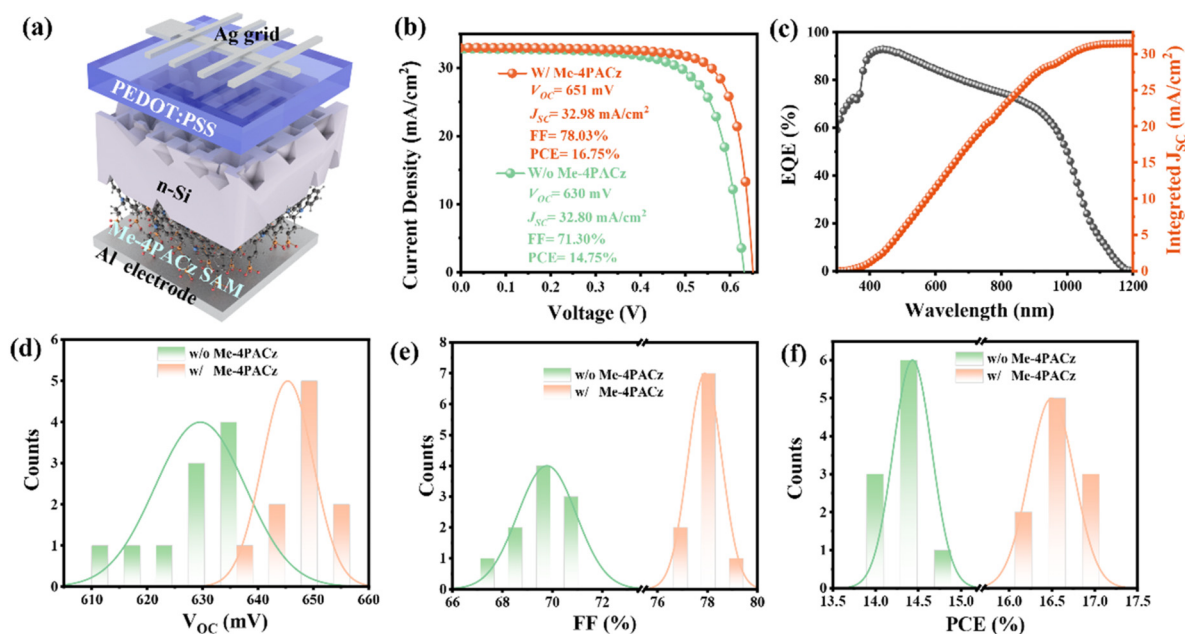
FIG. 4. (a) The device structure of PEDOT:PSS/Si solar cells with Me-4PACz/Al as an electronic selective contact. (b) $J–V$ and (c) external quantum efficiency (EQE) curves of champion devices with/without Me-4PACz SAM interlayers. Device performance statistics for PEDOT:PSS/Si solar cells with/without Me-4PACz interlayers. (d) V_{OC}, (e) FF, and (f) PCE for 10 independent devices each.

function of the Al electrode before and after modification ($\Delta\Phi = 0.31$ eV) remains consistent in both the KPFM and UPS systems, thereby confirming the reproducibility of the interface modification effect. Based on the aforementioned results, a band structure model of the n-Si/Al interface was established, as depicted in Fig. 3(e). The orientation of the dipole layer (relatively positive phosphonic acid group bound to c-Si, relatively negative carbazole group facing Al) generates a built-in electric field pointing from Al to c-Si [Fig. 3(e)]. This built-in electric field simultaneously: (i) lowers the effective work function of the Al electrode (confirmed by KPFM/UPS), reducing the electron Schottky barrier height (δ_n), and (ii) induces downward band bending in the n-Si conduction band near the interface. As a result, the energy barrier for electron transport from c-Si to Al is significantly diminished, facilitating efficient Ohmic extraction of electrons.

Figure 4(a) presents a schematic diagram of the device structure of a PEDOT:PSS/Si solar cell featuring a SAM-modified layer of Me-4PACz type. The concentration of Me-4PACz was optimized by preparing solutions with varying molar ratios, which ranged from 0 to 1.1 mM. As depicted in Figs. S5 and S6, along with Table S1, the highest PCE of 16.75% was attained at 0.8 mM, while concentrations exceeding 1.1 mM led to a reduction in PCE. Unless otherwise stated, the optimal concentration was employed for all SAM-modified devices and samples. The photovoltaic performance of n-Si/PEDOT:PSS solar cells with/without Me-4PACz interlayers was systematically evaluated under AM 1.5G illumination. As shown in Fig. 4(b), the control device (without Me-4PACz) achieved a PCE of 14.75% ($V_{OC} = 630$ mV, $J_{SC} = 32.80$ mA/cm^2, and FF = 71.30%). With Me-4PACz modification, the PCE increased to 16.75%, driven by concurrent improvements in V_{OC} (651 mV), J_{SC} (32.98 mA/cm^2), and FF (78.03%). These results surpass most reported PEDOT:PSS/nanostructured Si hybrid solar cells in V_{OC} and FF, as shown in Table S2. The *EQE* curve of the PEDOT:PSS/Si solar cell based on the SAM interlayer is depicted in Fig. 4(c). Integration of the *EQE* spectra yielded a J_{SC} of 31.45 mA/cm^2, consistent with the J–V measurement, validating the reliability of the data.

Statistical analysis of the performance of the two devices shows that the Me-4PACz modified device outperforms the control device in all photovoltaic indicators [Figs. 4(d)–4(f)]. This is attributed to the Me-4PACz with a high dipole moment, which induces a strong built-in electric field at the c-Si/Al interface and reduces the contact resistivity to 4.12 mΩ cm^2, thereby enhancing the ability of interface electron extraction and transport.

In this work, we demonstrate that molecular engineering of the c-Si/Al interface with a carbazole-based self-assembled monolayer (Me-4PACz) effectively alleviates carrier transport limitations in PEDOT:PSS/Si hybrid solar cells. The directional dipole moment introduced by Me-4PACz generates a strong built-in electric field, which establishes an Ohmic contact with a low resistivity (4.12 mΩ cm^2). Consequently, the optimized dopant-free PEDOT:PSS/Si hybrid solar cell achieved a PCE of 16.75%, with a V_{OC} of 651 mV and an FF of 78.03%. This study demonstrates SAMs as an effective strategy for interfacial carrier transport regulation in silicon-based solar cells.

See the supplementary material for experimental methods, XPS spectra of N 1s and P 2p, contact angle, AFM images, J–V curves, and photovoltaic parameter statistics of PEDOT:PSS/Si solar cells with different concentrations of the SAM interlayer.

AUTHOR DECLARATIONS
Conflict of Interest

The authors have no conflicts to disclose.

Author Contributions

Zhangbo Lu: Conceptualization (equal); Formal analysis (equal); Funding acquisition (equal); Project administration (equal); Resources (equal); Supervision (equal); Writing – original draft (equal); Writing – review & editing (equal). **Jiahui Chen:** Data curation (equal); Methodology (equal). **Yueyue Wu:** Data curation (equal); Methodology (equal). **Huanyu Wen:** Investigation (supporting). **Dan Chi:** Investigation (supporting). **Shihua Huang:** Project administration (equal); Resources (equal); Supervision (equal).

DATA AVAILABILITY

The data that support the findings of this study are available from the corresponding author upon reasonable request.

REFERENCES

[1]H. Wu, F. Ye, M. Yang, F. Luo, X. Tang, Q. Tang, H. Qiu, Z. Huang, G. Wang, Z. Sun, H. Lin, J. Wei, Y. Li, X. Tian, J. Zhang, L. Xie, X. Deng, T. Yuan, M. Yu, Y. Liu, P. Li, H. Chen, S. Zhou, Q. Xu, P. Li, J. Duan, J. Chen, C. Li, S. Yin, B. Liu, C. Sun, Q. Su, Y. Wang, H. Deng, T. Xie, P. Gao, Q. Kang, Y. Zhang, H. Yan, N. Yuan, F. Peng, Y. Yuan, X. Ru, B. He, L. Chen, J. Wang, J. Lu, M. Qu, C. Xue, J. Ding, L. Fang, Z. Li, and X. Xu, Nature **635**(8039), 604–609 (2024).

[2]G. Wang, Q. Su, H. Tang, H. Wu, H. Lin, C. Han, T. Wang, C. Xue, J. Lu, L. Fang, Z. Li, X. Xu, and P. Gao, Nat. Commun. **15**(1), 8931 (2024).

[3]B. Sun, M. Shao, and S. Lee, Adv. Mater. **28**(47), 10539–10547 (2016).

[4]P. Gao, Z. Yang, J. He, J. Yu, P. Liu, J. Zhu, Z. Ge, and J. Ye, Adv. Sci. **5**(3), 1700547 (2017).

[5]M. F. Abdelbar, M. Abdelhameed, M. Esmat, M. El-Kemary, and N. Fukata, Nano Energy **89**, 106470 (2021).

[6]Z. Sun, M. Liu, J. Zhou, Q. Wang, Y. Yang, Y. Zhou, and F. Liu, Sol. Energy Mater. Sol. Cells **235**, 111453 (2022).

[7]S. S. Yoon and D. Y. Khang, Adv. Energy Mater. **8**(9), 1702655 (2018).

[8]Z. Sun, Y. He, B. Xiong, S. Chen, M. Li, Y. Zhou, Y. Zheng, K. Sun, and C. Yang, Angew. Chem. Int. Ed. **60**(10), 5036–5055 (2021).

[9]R. Shen, Z. Sun, Y. Shi, Y. Zhou, W. Guo, Y. Zhou, H. Yan, and F. Liu, ACS Nano **15**(4), 6296–6304 (2021).

[10]R. Shen, Z. Sun, Y. Zhou, Y. Shi, J. Shang, H. Chen, Y. Zhou, and F. Liu, Prog. Photovoltaics. Res. Appl. **30**(6), 661–669 (2022).

[11]S. B. Kang, W. J. Park, M. H. Jeong, S. H. Kang, C. Yang, and K. J. Choi, Adv. Funct. Mater. **30**(50), 2004943 (2020).

[12]Y. Wan, S. K. Karuturi, C. Samundsett, J. Bullock, M. Hettick, D. Yan, J. Peng, P. R. Narangari, S. Mokkapati, H. H. Tan, C. Jagadish, A. Javey, and A. Cuevas, ACS Energy Lett. **3**(1), 125–131 (2018).

[13]K. Gao, Q. Bi, X. Wang, W. Liu, C. Xing, K. Li, D. Xu, Z. Su, C. Zhang, J. Yu, D. Li, B. Sun, J. Bullock, X. Zhang, and X. Yang, Adv. Mater. **34**(26), 2200344 (2022).

[14]T. Matsui, S. Fukaya, S. McNab, J. McQueen, K. Gotoh, H. Sai, N. Usami, and R. S. Bonilla, Adv. Sci. **12**(3), 2410179 (2024).

[15]C. Xing, W. Gu, Z. Xiang, X. Lou, K. Wang, X. Zhang, Y. Wang, X. Yang, and B. Sun, Chem. Eng. J. **481**, 148568 (2024).

[16]D. Xu, Q. Bi, K. Li, K. Gao, X. Wang, W. Shi, S. Wang, C. Xing, X. Zhang, and X. Yang, Adv. Funct. Mater. **34**(44), 2407290 (2024).

[17]Y. Zhang, T. Shi, L. Duan, B. Hoex, and Z. Tang, Nano Energy **131**, 110282 (2024).

[18]J. Zhao, Z. Zhang, S. Xie, F. Liu, Y. Zhen, S. Li, W. Liu, A. Han, L. Zhang, Z. Liu, Y. Sun, and W. Liu, Chem. Eng. J. **498**, 155656 (2024).

[19]H. Tang, Z. Shen, Y. Shen, G. Yan, Y. Wang, Q. Han, and L. Han, Science **383**(6688), 1236–1240 (2024).

[20]J. Suo, B. Yang, D. Bogachuk, G. Boschloo, and A. Hagfeldt, Adv. Energy Mater. **15**(2), 2400205 (2025).

[21]Y. An, N. Zhang, Q. Liu, W. Jiang, G. Du, D. Chen, M. Liu, X. Huang, T. Lei, Q. Qiu, F. R. Lin, X. C. Zeng, A. K. Y. Jen, and H.-L. Yip, Nat. Commun. **16**(1), 2759 (2025).

[22]C. Guo, H. Q. Du, Y. C. Wang, X. Gao, Y. Q. Lan, Y. S. Xiao, W. Jiang, Y. C. Zhou, Q. B. Yuan, Z. Y. Qiang, J. H. Zheng, L. H. Yang, C. X. Wang, N. Yang, R. Lin, G. J. Liang, M. U. Rothmann, X. Ouyang, Y. B. Cheng, and W. Li, Adv. Mater. **37**, 2504520 (2025).

[23]T. Liu, C. Luo, R. He, Z. Zhang, X. Lin, Y. Chen, and T. Wu, Adv. Mater. 2502032 (2025).

[24]X. Zhang, Y. Wang, K. Zhang, M. Tao, H. Guo, L. Guo, Z. Song, J. Wen, Y. Yang, Y. Hou, and Y. Song, Angew. Chem. Int. Ed. **64**(13), e202423827 (2025).

[25]Z. Su, B. Yu, Y. Sun, J. Zhang, and H. Yu, Appl. Phys. Lett. **125**(24), 243902 (2024).

[26]J. Burger, V. Papaioannou, S. Gopinath, G. Jackson, A. Galindo, and C. S. Adjiman, AIChE J. **61**(10), 3249–3269 (2015).

[27]R. Deschermeier, S. Rehfeldt, and H. Klein, Chem. Eng. Technol. **40**(1), 28–38 (2017).

[28]P. Canepa, G. Gonella, G. Pinto, V. Grachev, M. Canepa, and O. Cavalleri, J. Phys. Chem. C **123**(27), 16843–16850 (2019).

[29]G. K. Reeves and H. B. Harrison, IEEE Electron Device Lett. **3**(5), 111–113 (1982).

[30]K. Carter-Fenk and J. M. Herbert, Phys. Chem. Chem. Phys. **22**(43), 24870–24886 (2020).

[31]C. Li, Y. Chen, Y. Li, L. Gong, Z. Yuan, L. Liang, J. Chen, P. Ganesan, Y. Zhang, J. Ma, and P. Gao, Angew. Chem. Int. Ed. **64**(9), e202420585 (2025).

[32]Z. Yang, P. Gao, J. Sheng, H. Tong, C. Quan, X. Yang, K. W. A. Chee, B. Yan, Y. Zeng, and J. Ye, Nano Energy **46**, 133–140 (2018).

[33]W. Ji, T. Allen, X. Yang, G. Zeng, S. De Wolf, and A. Javey, ACS Energy Lett. **5**(3), 897–902 (2020).

[34]K. Gao, C. Xing, D. Xu, X. Lou, X. Wang, K. Li, W. Li, J. Mao, P. Zheng, X. Zhang, and X. Yang, Small **20**(29), 2310352 (2024).

Supporting Information

Dipole engineering in self-assembled monolayers for efficient organic–silicon hybrid solar cells

Zhangbo Lu[a], Jiahui Chen, Yueyue Wu, Huanyu Wen, Dan Chi, Shihua Huang[a]

Key Laboratory of Solid State Optoelectronic Devices of Zhejiang Province, College of Physics and Electronic Information Engineering, Zhejiang Normal University, Jinhua 321004, China

[a]Author to whom correspondence should be addressed: luzhangbo@zjnu.edu.cn and huangshihua@zjnu.cn.

1. Experimental section

2.1. Preparation of Nanostructured Si

Single sided polished <100> oriented n-type n-Si substrate (thickness of 500 μm) was used for the preparation of PEDOT: PSS/Si photovoltaic devices. Silicon wafers are pre-cleaned successively through boiling acid (with a volume ratio of HCl: H_2O_2: H_2O being 1:2:5) and boiling alkali (with a volume ratio of $NH_3 \cdot H_2O$: H_2O_2: H_2O being 1:2:6) solutions. Subsequently, the cleaned Si substrates were immersed in an

etching solution composed of 0.2 mol L^{-1} silver nitrate (AgNO$_3$, AR, ≥99.8%), 50 mL of 40 wt% hydrofluoric acid (HF AR, ≥40.0%), and 130 mL of deionized water for 5 minutes. After etching, the wafers were thoroughly rinsed with deionized water. Afterwards, they were immersed in HNO$_3$ solution and 10 wt% HF aqueous solution for 10 min to remove Ag residues and SiO$_x$ layer, respectively. Finally, the Si NWs substrates were etched with 1 wt% TMAH aqueous solution for 60 seconds, thereby obtaining nanostructured Si.

2.2. Device fabrication

The PEDOT:PSS solution (Clevios™ PH1000) was doped with 5 wt% dimethyl sulfoxide and 1 wt% Triton™ X-100 surfactant under continuous magnetic stirring for 1 hour. The modified solution was spin-coated onto the nanostructured silicon substrates at 3000 rpm for 30 s, followed by thermal annealing at 120 °C for 20 minutes in ambient air. Finally, front and rear electrodes were deposited via thermal evaporation: a 500 nm-thick Ag grid top electrode and a 500 nm-thick Al back electrode. The active area of the hybrid solar cells was defined as 0.5 cm² using a shadow mask.

2.3. Device characterization

The atomic composition and chemical states of the n-Si/SAM film were analyzed using X-ray photoelectron spectroscopy (XPS, K-Alpha, Thermo Fisher) with monochromatic Al Kα X-ray. Ultraviolet photoelectron spectroscopy (UPS) measurements were performed using a Thermo Scientific™ ESCALAB 250XI system (equipped with a He Iα excitation source, hν=21.2 eV) to determine the work function.

The Kelvin probe force microscopy (KPFM) measurements were carried out in air conditions (Bruker Dimension ICON) using frequency-modulation KPFM to probe the contact potential difference (CPD) between the n-Si/Ti or n-Si/Me-4PACz/Ti surface and the tip. The measurement of contact resistance was conducted by employing a solar cell TLM method grid line contact resistance analyzer of model Ai-TLM-04. The current density-voltage (J-V) characteristics of PEDOT:PSS/Si devices were measured by a solar simulator (Sol3A, Newport) under AM 1.5 illumination (1000 W m^{-2}) standard test conditions. The external quantum efficiency (EQE) spectra were measured in the wavelength range 300–1200 nm with the QEX-10 measuring system.

2.4. Computational Details

The theoretical calculations were performed via the Gaussian 16 suite of programs[1]. The structure of the studied molecule was fully optimized at the B3LYP-D3BJ/6-31G(d) level of theory. The solvent effect was included in the calculations using the solvation model based on the density (SMD) model[2]. The vibrational frequencies of the optimized structure were carried out at the same level. The structures were characterized as a local energy minimum on the potential energy surface by verifying that all the vibrational frequencies were real. The dipole moment of the molecule was calculated with a larger basis set def2-TZVPD basis set. The Visual Molecular Dynamics (VMD) program[3] was used to plot the color-filled iso-surface graphs to visualize the molecular electrostatic potential (MESP).
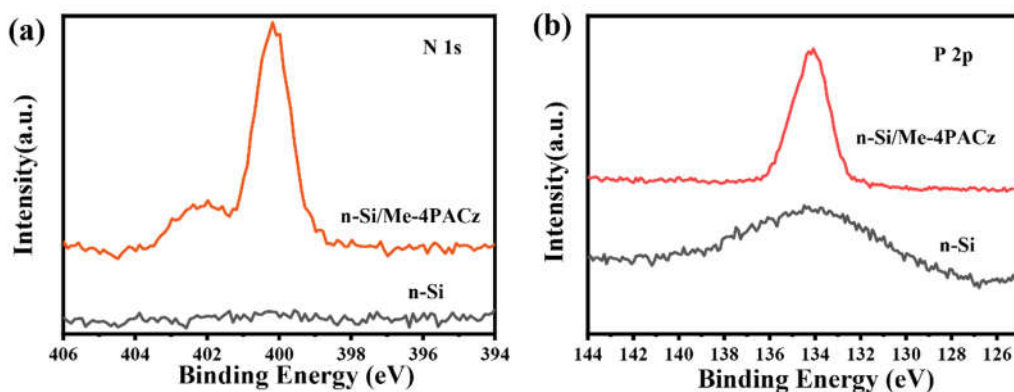
Figure S1. High-resolution XPS spectra for (a) N 1s and (b) P 2p without and with

Me-4PACz. The broad and weak peak of high-resolution P 2p is related to the trace P

element doped in n-Si, while the sharp and strong peak observed after Me-4PACz spin

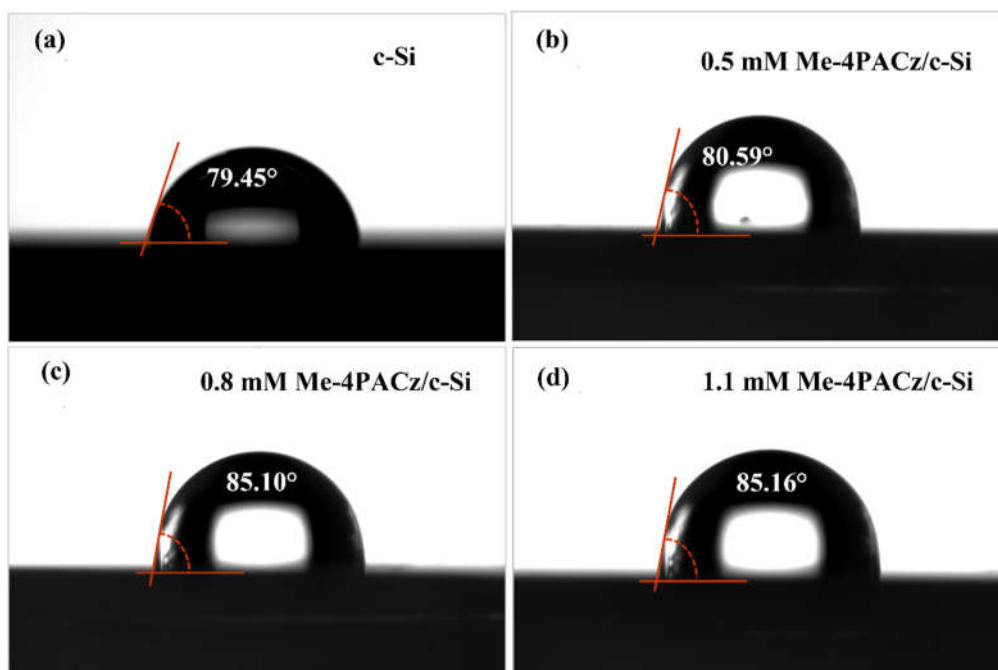coating onto n-Si is related to the phosphate groups in the self-assembled monolayer.

Figure S2. (a) Contact angles of c-Si and (b, c, d) c-Si/SAM with different
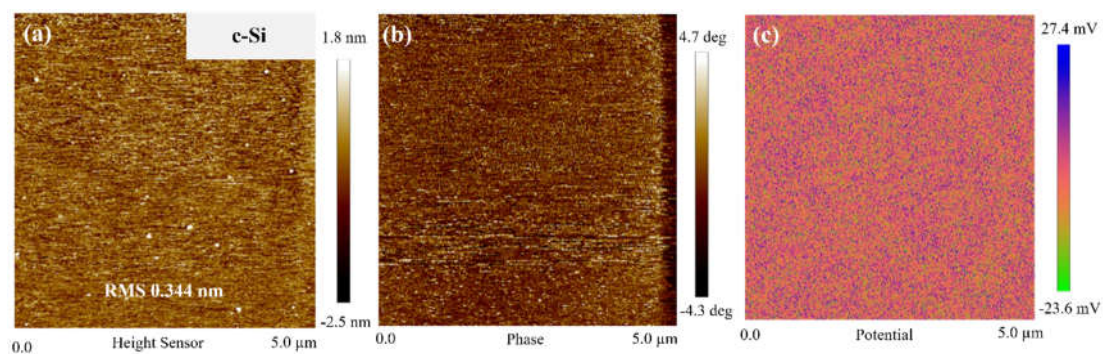
concentrations of Me-4PACz (0.5, 0.8, 1.1 mM).

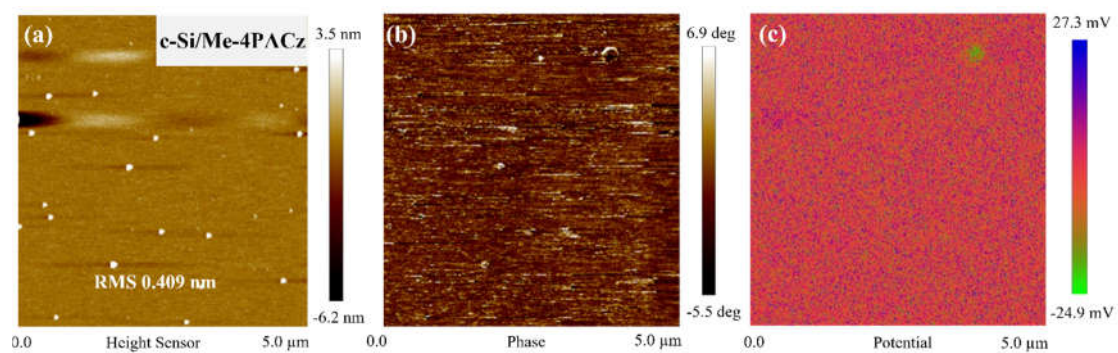**Figure S3.** Top-view (a) topography, (b) phase, and (c) potential of polished n-Si.

Figure S4. Top-view (a) topography, (b) phase, and (c) potential of polished n-Si/Me-4PACz.
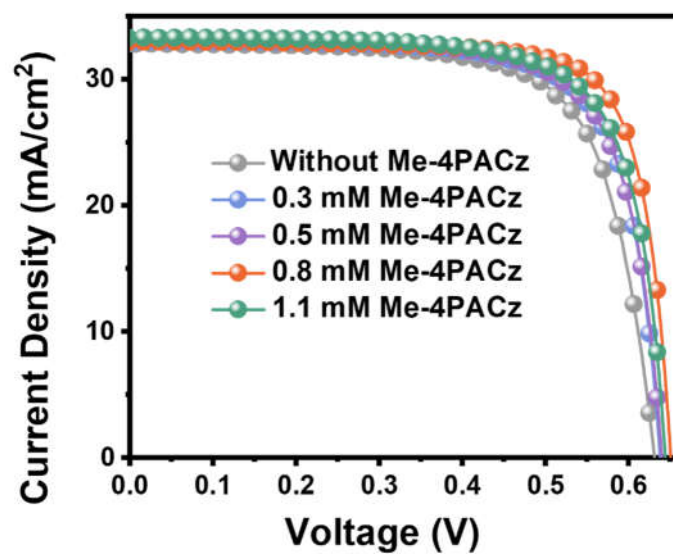
Figure S5. *J-V* curves of champion devices based on different concentrations of SAM ESCs.
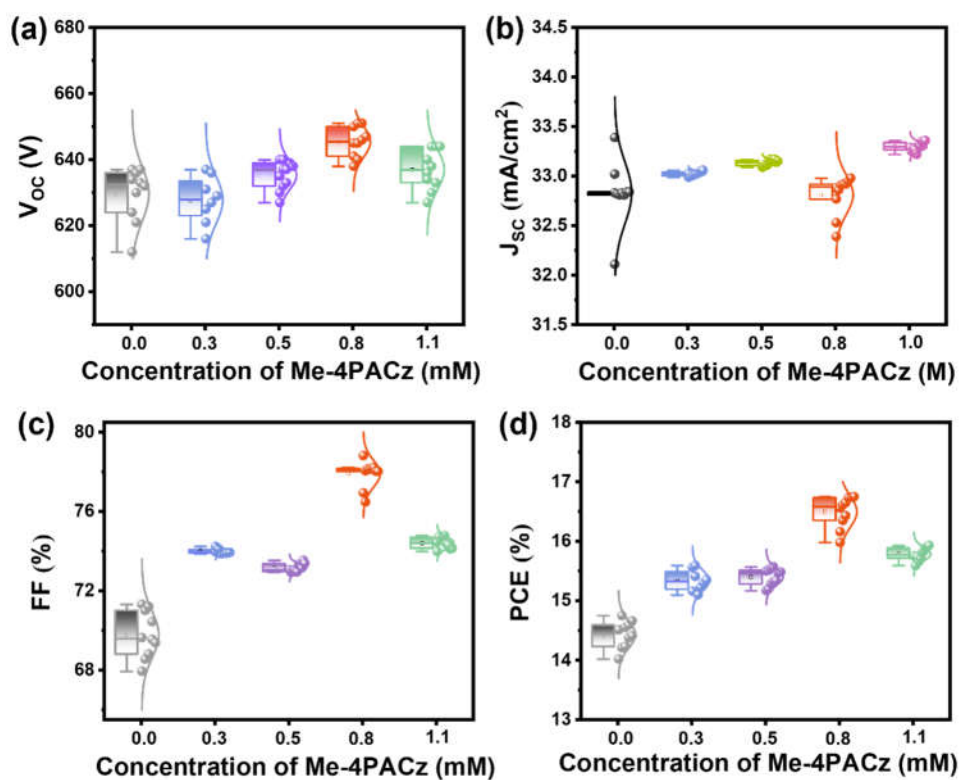

Figure S6. Performance comparison between PEDOT:PSS/n-Si solar cells based on Me-4PACz ESCs with different molar concentrations (Approximately 10 devices per concentration).

Table S1. Photovoltaic parameters of champion devices based on different concentrations of Me-4PACz ESCs.

Devices	V_{OC} (V)	J_{SC} (mA/cm²)	FF (%)	PCE (%)
w/o Me-4PACz	630	32.80	71.30	14.75
0.3 M Me-4PACz	637	33.05	73.94	15.56
0.5 M Me-4PACz	639	33.15	73.37	15.57
0.8 M Me-4PACz	651	32.98	78.03	16.75
1.0 M Me-4PACz	644	33.35	74.14	15.93

Table S2. Previous reports on high performance PEDOT:PSS/nanostructured Si solar cells with rear interface modification.

Devices	V_{OC} (V)	J_{SC} (mA/cm²)	FF (%)	PCE (%)	Ref.
SiO_X+Mg/ Pyramidal Si	610	33.40	73.50	15.00	4
TEOS/ Nanostructure Si	622	33.50	78.00	16.30	5
TiO_X+LiF_X/ Pyramid Si	626	31.90	75.60	15.10	6
CPTA/Pyramid Si	632	34.70	76.30	16.73	7
Siloxane/ Hierarchical Si	610	38.41	74.00	17.34	8
P(VDF-TrFE)/ Cone-shaped Si	645	37.72	75.50	18.37	9
SAM/Inverted pyramid Si	651	32.98	78.03	16.75	This work

REFERENCES

[1]M. J. Frisch, G. W. Trucks, H. B. Schlegel, G. E. Scuseria, M. A. Robb, J. R. Cheeseman, et al., Gaussian 16, Revision A.03; Gaussian, Inc.: Wallingford, CT, 2016.

[2]A. V. Marenich, C. J. Cramer, and D. G. Truhlar, J. Phys. Chem. B 113, 6378 (2009).

[3]W. Humphrey, A. Dalke, and K. Schulten, J. Mol. Graph. Model. 14, 33 (1996).

[4]H. Tong, Z. Yang, X. Wang, Z. Liu, Z. Chen, X. Ke, M. Sui, J. Tang, T. Yu, Z. Ge, Y. Zeng, P. Gao, and J. Ye, Adv. Energy Mater. **8** (16), 1702921 (2018).

[5]Z. Xia, P. Gao, T. Sun, H. Wu, Y. Tan, T. Song, S.-T. Lee, and B. Sun, ACS Appl. Mater. Interfaces **10** (16), 13767−13773 (2018).

[6]J. He, M. A. Hossain, H. Lin, W. Wang, S. K. Karuturi, B. Hoex, J. Ye, P. Gao, J. Bullock, and Y. Wan, ACS Nano **13** (6), 6356−6362 (2019).

[7]J. He, Y. Wan, P. Gao, J. Tang, and J. Ye, Adv. Funct. Mater. **28** (34), 1802192 (2018).

[8]S. S. Yoon and D. Y. Khang, Adv. Energy Mater. **8** (9), 1702655 (2017).

[9]S. B. Kang, W. J. Park, M. H. Jeong, S. H. Kang, C. Yang, and K. J. Choi, Adv. Funct. Mater. **30** (50), 2004943 (2020).